HIGH-RESOLUTION X-RAY SPECTROSCOPY OF THE POST–T TAURI STAR PZ TELESCOPII

C. Argiroffi,[1] J. J. Drake,[2] A. Maggio,[3] G. Peres,[1] S. Sciortino,[3] and F. R. Harnden[2]

ABSTRACT

We present an analysis of the *Chandra* High Energy Transmission Grating Spectrometer observation of the rapidly rotating ($P_{\rm rot} = 0.94$ days) post–T Tauri ($\sim$20 Myr old) star PZ Telescopii, in the Tucana association. Using two different methods, we have derived the coronal emission measure distribution EM(T) and chemical abundances. The EM(T) peaks at $\log T = 6.9$ and exhibits a significant emission measure at temperatures $\log T > 7$. The coronal abundances are generally $\sim$0.5 times the solar photospheric values, which are presumed fairly representative of the composition of the underlying star. A minimum in abundance is seen at a first ionization potential (FIP) of 7–8 eV, with evidence for higher abundances at both lower and higher FIP, similar to patterns seen in other active stars. From an analysis of the He-like triplet of Mg XI, we have estimated electron densities of $\sim10^{12}$–10^{13} cm^{-3}. All the coronal properties found for PZ Tel are much more similar to those of AB Dor, which is slightly older than PZ Tel, than to those of the younger T Tauri star TW Hya. These results support earlier conclusions that the soft X-ray emission of TW Hya is likely dominated by accretion activity rather than by a magnetically heated corona. Our results also suggest that the coronae of pre–main-sequence stars rapidly become similar to those of older active main-sequence stars soon after the accretion stage has ended.

Subject headings: stars: abundances — stars: coronae — stars: individual (PZ Telescopii) —
stars: pre–main-sequence — techniques: spectroscopic — X-rays: stars

1. INTRODUCTION

One of the primary characteristics of low-mass pre–main-sequence (PMS) stars is their intense X-ray activity. This X-ray emission therefore represents an important means for investigating the properties and evolution of young stellar objects. X-ray activity is present during the evolution of PMS stars both in the initial evolutionary stages of a classic T Tauri star (CTTS, Class I and II sources), during which the star has an accretion disk that surrounds it, and in the subsequent weak-line T Tauri star (WTTS, Class III sources) phase, in which the star has no accreting material and is approaching the zero-age main sequence (ZAMS; Feigelson & Montmerle 1999). How the presence of accreting material influences the X-ray emission of PMS stars, and for how long, remain questions of debate.

The high-resolution X-ray spectra now available with the *Chandra* and *XMM-Newton* satellites offer the possibility of performing detailed studies of stellar coronae because the diagnostics of key emission lines can now be resolved. These diagnostics can be used to derive the elemental abundances, temperature, and density structure of the emitting plasmas.

It is worth noting that very few young stars in star-forming regions or associations are sufficiently X-ray bright to allow high-resolution X-ray spectroscopy with current instrumentation. In particular, among the CTTSs TW Hya is the best-studied case to date because it is the nearest ($\sim$56 pc) known CTTS. TW Hya shows spectral characteristics very different from those of young but otherwise *normal* active stars (Kastner et al. 2002; Stelzer & Schmitt 2004): very low

plasma temperature ($\log T \sim 6.5$), high density ($\log N_e \sim 13$), and very low Fe abundance ($A_{\rm Fe}/A_{\rm Fe_\odot} \sim 0.2$). Kastner et al. (2002) and Stelzer & Schmitt (2004) attributed these characteristics to an accretion shock rather than coronal activity. Without the benefit of high-resolution spectra of similar stars for comparison, however, the nature of the peculiarity of TW Hya remains uncertain.

The situation with slightly more evolved stars is more clear. Studies of AB Dor, a young active star that has nearly arrived at the ZAMS and that has been observed in the past with several space-borne X-ray observatories, have shown that it is characterized by a hot corona ($T \sim 10^7$ K), with plasma densities ranging from 6×10^{10} cm^{-3} at 2×10^6 K to 3×10^{12} cm^{-3} at 10^7 K, and a moderately low Fe abundance ($A_{\rm Fe}/A_{\rm Fe_\odot} \sim 0.25$; Mewe et al. 1996; Güdel et al. 2001; Sanz-Forcada et al. 2003b; P. Testa 2004, in preparation; D. García-Alvarez 2004, in preparation). In many respects, AB Dor can be considered the prototype of very active single stars.

High-resolution X-ray spectroscopy of other PMS stars with ages between a few 10^6 yr, typical of CTTSs such as TW Hya, and 10^8 yr, the ZAMS of solar-type stars such as AB Dor, is crucial for understanding how the characteristics of stellar X-ray activity change during these early evolutionary phases.

In this work, we present a *Chandra* High Energy Transmission Grating Spectrometer (HETGS) observation of PZ Telescopii (HD 174429, HIP 92680). Classified as a K0 V star by Houk (1978), PZ Tel was determined by Zuckerman & Webb (2000) to be a member of the Tucana association, a nearby star-forming region $\sim$45 pc away. From observations with the *ROSAT* PSPC, Stelzer & Neuhäuser (2000) deduced a PZ Tel X-ray luminosity of $L_X \sim (2.88 \pm 0.08) \times 10^{30}$ ergs s^{-1}. At a *Hipparcos* parallax distance of 49.7 ± 2.9 pc (Perryman et al. 1997), PZ Tel is a single star with a rotational period of 0.94 days (Coates et al. 1980; Innis et al. 1984, 1986). Favata et al. (1998) have estimated a mass of 1.1 $M_\odot$ for PZ Tel and an age of approximately 20 Myr. Its youth is also confirmed by prominent Hα emission and a relatively

[1] Dipartimento di Scienze Fisiche ed Astronomiche, Sezione di Astronomia, Università di Palermo, Piazza del Parlamento 1, 90134 Palermo, Italy; argi@astropa.unipa.it, peres@astropa.unipa.it.

[2] Smithsonian Astrophysics Observatory, 60 Garden Street, Cambridge, MA 02138; jdrake@cfa.harvard.edu, frh@cfa.harvard.edu.

[3] INAF - Osservatorio Astronomico di Palermo, Piazza del Parlamento 1, 90134 Palermo, Italy; maggio@astropa.unipa.it, sciorti@astropa.unipa.it.

undepleted Li abundance (Soderblom et al. 1998). Further evidence of its PMS status has been pointed out by Barnes et al. (2000), who deduced from $v \sin i$ and P_{rot} that the minimum radius of PZ Tel is $R \sin i \sim 1.27\ R_{\odot}$: this value is larger than the radius of a main-sequence star with the same mass as PZ Tel.

The analysis of *Chandra* HETGS high-resolution spectra of PZ Tel offers us the opportunity to study the coronal properties of a single star that has dissipated its accretion disk and is approaching the ZAMS. This study also allows us to compare the coronal properties of PZ Tel with those of both younger and older stars, providing a glimpse of the evolution of stellar coronae through the PMS phase. In particular, the CTTSs have disks from which active accretion is still taking place. These stars could have quite different magnetospheric geometries, possibly involving magnetic connections between star and disk (e.g., Montmerle 2002). In the case of coeval and older stars, it appears that the coronal activity of PMS stars without an accreting disk can be explained on the same basis as that of main-sequence stars (Flaccomio et al. 2003): stellar rotation and convection. In this domain, PZ Tel provides a new window on phenomena such as the chemical fractionation of elements that is seen to occur in coronae over a wide range of activity level. In the solar case, elements with low first ionization potential (FIP) such as Mg, Fe, and Si are seen to be enhanced relative to elements with high FIP such as O, Ne, and Ar (e.g., Feldman 1992). In more active stars the situation appears somewhat reversed, with elements such as Ne appearing enhanced relative to those with lower FIP (e.g., Drake 2002 and references therein). The case of the active but very young post–T Tauri stars remains unexplored at high spectral resolution.

In §§ 2 and 3, we describe the *Chandra* observation and the techniques used in its analysis. In § 4, we present the resulting coronal temperature structure and abundances. These are discussed in § 5, in which we also present a comparison of the coronal properties of PZ Tel with those of AB Dor and TW Hya.

2. OBSERVATION

PZ Tel was observed with the *Chandra* HETGS on 2003 June 7 for 73.9 ks. The HETGS provides both high-energy grating (HEG) and medium-energy grating (MEG) spectra. The spectral ranges available with these instruments are 1–18 (HEG) and 1–25 Å (MEG), with spectral resolutions $\Delta\lambda$ of 0.01 and 0.02 Å, respectively. We have used CIAO version 3.0 to extract the positive and negative first-order spectra for each grating and to compute the effective area of the HETG + ACIS-S combinations. In this latter step, we have also taken into account the attenuation resulting from the buildup of a contamination layer on the ACIS-S filter (e.g., Plucinsky et al. 2003) using version 1 of the CIAO effective area contamination correction.[4] In Figure 1, we show the light curve of photon arrival times of the HEG and MEG spectra, excluding zeroth-order events that are subject to significant pileup. Figure 1 shows the X-ray flux to be characterized by variability on timescales of a few to tens of ks, with two flare-like events occurring at ~20 and 55 ks after the start of the observation.

In Figure 2, we illustrate the first-order MEG spectrum; labels identify the strongest emission lines. The X-ray luminos-

---

[4] The CIAO ver. 3.0 Web site on correcting ACIS contamination is at http://cxc.harvard.edu/ciao/threads/aciscontam.
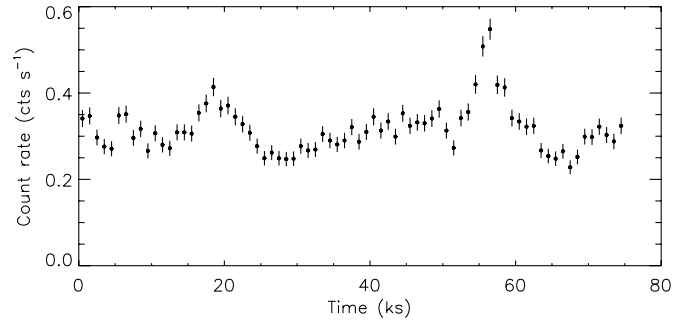

FIG. 1.—Light curve of PZ Tel obtained from the HEG and MEG spectra (excluding zeroth-order events) with bin size of 1000 s.

ity obtained from the first-order dispersed events in the interval 6–20 Å is $L_X = 2.2 \times 10^{30}$ ergs s^{-1}, from which we derive $\log (L_X/L_{bol}) = -3.2$, having adopted $L_{bol} = 3.6 \times 10^{33}$ ergs s^{-1} (obtained from the m_V and $B-V$ *Hipparcos* data and the bolometric correction of Flower 1996).

3. ANALYSIS

The MEG first-order spectrum has more than 1.6×10^4 total counts and contains lines with good signal-to-noise ratios (S/Ns). The HEG spectrum consists of 5.5×10^3 counts, with few lines having sufficient counts to provide useful fluxes. We have therefore based our analysis on the MEG spectrum only. The MEG background is extremely low and contains an average of only 0.02 counts per ACIS pixel and was therefore ignored.

The spectral analysis of PZ Tel has been performed using the PINTofALE version 1.5 software package (Kashyap & Drake 2000). We have adopted the CHIANTI version 4 emission-line database (Young et al. 2003) and the Mazzotta et al. (1998) ionization equilibrium.

Spectral line fluxes were obtained by fitting the counts histograms with a modified Lorentzian profile of the type

$$I(\lambda) = I_{max}\left[1 + \left(\frac{\lambda - \lambda_0}{\Delta\lambda}\right)^2\right]^{-\beta},$$

with $\beta = 2.4$, plus a piecewise constant continuum level. For the continuum placement, we have adopted the following procedure. As a first step we have guessed an emission measure distribution EM(T) and set of abundances in order to predict a continuum level for measuring line fluxes. From these line fluxes, we evaluated the EM(T) and abundances for PZ Tel and updated the predicted continuum level. Considering this new predicted continuum, we have once again measured the line fluxes. We performed several iterations of the above procedure until convergence, i.e., until the continuum used for the line fitting agrees with the continuum predicted on the basis of the reconstructed EM(T) and computed abundances.

In Table 1, we report the strongest lines identified in the PZ Tel spectrum together with their measured MEG count rates. As stated in § 2, significant variability of the X-ray emission occurred during the observation, but the MEG S/N did not allow us to perform time-resolved spectral analysis of the data. On the other hand, the integrated PZ Tel spectrum provides a good representation of the average state of an active corona where a low-level flarelike activity is present at all times.
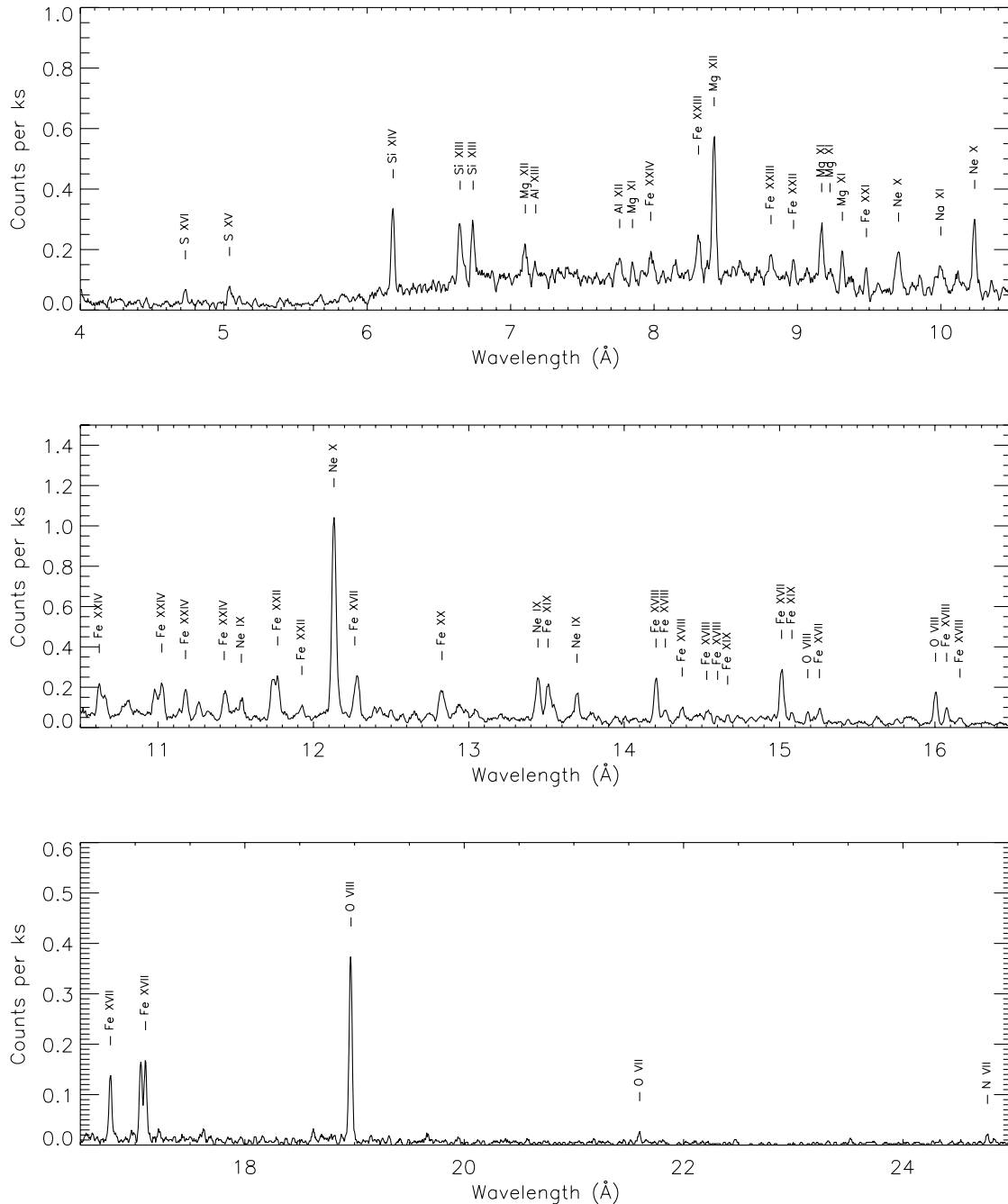
Fig. 2.—PZ Tel MEG smoothed spectrum (summed positive and negative orders) with bin size of 0.005 Å.

The hydrogen column density toward PZ Tel is not known, and there is insufficient information in the HETG spectrum to estimate it. For all the following analyses we have therefore assumed a hydrogen column density of 10^{19} cm^{-2}, appropriate for the distance of PZ Tel (49.7 pc) and an average interstellar medium density of 0.1 cm^{-3}. We have estimated that if the hydrogen column density is as high as 10^{20} cm^{-2}, the effect would be marginally observable only for the O and N lines at $\lambda > 18$ Å, with an absorption of ~5%–10%.

3.1. Emission Measure Distribution and Abundance Reconstruction

We have derived the emission measure distribution from individual line fluxes: one of the main advantages of this procedure in comparison with a global fitting approach is that we can use only the spectral information that we consider most reliable. This choice involves the question of which lines to include in the EM(T) reconstruction and which to exclude. In principle, one would expect that lines that form over the same temperature range should give consistent emission measure values and therefore different line selections should not provide significant differences in the final EM(T). However, in some cases the above assumption will not be correct because of uncertainties in the atomic data, hidden line blending, and other line-measurement difficulties.

We have explored two different choices of spectral lines, which we describe below. For both of these selections, we derived the emission measure distribution using the method

TABLE 1
MEG Spectrum of PZ Tel

Label	$\lambda_{\rm obs}$[a] (Å)	$\lambda_{\rm pred}$[a] (Å)	Ion	Transition (upper → lower)	$\log T_{\rm max}$[b] (K)	(Count Rates $\pm\ \sigma$)[c] (counts ks^{-1})	Effective Area[d] (cm^2)	EM(T)[e]
1a........	4.73	4.73	S XVI	$2p\ ^2P_{3/2} \rightarrow 1s\ ^2S_{1/2}$	7.40	0.30 ± 0.13	37.5	1, 2
1b........	...	4.73	S XVI	$2p\ ^2P_{1/2} \rightarrow 1s\ ^2S_{1/2}$	7.40	...	...	...
2..........	5.04	5.04	S XV	$1s\ 2p\ ^1P_1 \rightarrow 1s^2\ ^1S_0$	7.20	0.25 ± 0.12	35.2	1, 2
3a........	6.18	6.18	Si XIV	$2p\ ^2P_{3/2} \rightarrow 1s\ ^2S_{1/2}$	7.20	1.56 ± 0.22	99.7	1, 2
3b........	...	6.19	Si XIV	$2p\ ^2P_{1/2} \rightarrow 1s\ ^2S_{1/2}$	7.20	...	...	...
4..........	6.65	6.65	Si XIII	$1s\ 2p\ ^1P_1 \rightarrow 1s^2\ ^1S_0$	7.00	1.20 ± 0.22	117.4	1, 2
5a........	6.68	6.69	Si XIII	$1s\ 2p\ ^3P_2 \rightarrow 1s^2\ ^1S_0$	6.95	0.31 ± 0.17	118.1	...
5b........	...	6.69	Si XIII	$1s\ 2p\ ^3P_1 \rightarrow 1s^2\ ^1S_0$	6.95	...	...	...
6..........	6.74	6.74	Si XIII	$1s\ 2s\ ^3S_1 \rightarrow 1s^2\ ^1S_0$	7.00	1.14 ± 0.22	131.4	...
7a........	7.10	7.11	Mg XII	$3p\ ^2P_{3/2} \rightarrow 1s\ ^2S_{1/2}$	7.00	0.69 ± 0.19	145.5	...
7b........	...	7.11	Mg XII	$3p\ ^2P_{1/2} \rightarrow 1s\ ^2S_{1/2}$	7.00	...	...	...
8a........	7.18	7.17	Fe XXIV	$1s^2\ 5p\ ^2P_{3/2} \rightarrow 1s^2\ 2s\ ^2S_{1/2}$	7.30	0.21 ± 0.17	134.3	1, 2
8b........	...	7.17	Al XIII	$2p\ ^2P_{3/2} \rightarrow 1s\ ^2S_{1/2}$	7.10	...	...	...
8c........	...	7.18	Al XIII	$2p\ ^2P_{1/2} \rightarrow 1s\ ^2S_{1/2}$	7.10	...	...	...
9..........	7.76	7.76	Al XII	$1s\ 2p\ ^1P_1 \rightarrow 1s^2\ ^1S_0$	6.90	0.44 ± 0.18	132.9	1, 2
10........	7.85	7.85	Mg XI	$1s\ 3p\ ^1P_1 \rightarrow 1s^2\ ^1S_0$	6.80	0.23 ± 0.17	133.8	...
11a......	7.98	7.98	Fe XXIV	$1s^2\ 4p\ ^2P_{3/2} \rightarrow 1s^2\ 2s\ ^2S_{1/2}$	7.30	0.44 ± 0.18	131.4	1
11b......	...	7.99	Fe XXIV	$1s^2\ 4p\ ^2P_{1/2} \rightarrow 1s^2\ 2s\ ^2S_{1/2}$	7.30	...	...	...
12a......	8.31	8.30	Fe XXIII	$2s\ 4p\ ^1P_1 \rightarrow 2s^2\ ^1S_0$	7.20	0.93 ± 0.21	134.1	...
12b......	...	8.32	Fe XXIV	$1s^2\ 4d\ ^2D_{5/2} \rightarrow 1s^2\ 2p\ ^2P_{3/2}$	7.30	...	...	...
13a......	8.42	8.42	Mg XII	$2p\ ^2P_{3/2} \rightarrow 1s\ ^2S_{1/2}$	7.00	3.01 ± 0.29	136.7	1, 2
13b......	...	8.42	Mg XII	$2p\ ^2P_{1/2} \rightarrow 1s\ ^2S_{1/2}$	7.00	...	...	...
14........	8.82	8.81	Fe XXIII	$2s\ 4d\ ^1D_2 \rightarrow 2s\ 2p\ ^1P_1$	7.20	0.54 ± 0.19	125.1	...
15........	8.97	8.98	Fe XXII	$2s^2(^1S)4d\ ^2D_{3/2} \rightarrow 2s^2\ 2p\ ^2P_{1/2}$	7.10	0.35 ± 0.18	120.5	...
16........	9.17	9.17	Mg XI	$1s\ 2p\ ^1P_1 \rightarrow 1s^2\ ^1S_0$	6.80	1.42 ± 0.21	88.7	1, 2
17a......	9.23	9.23	Mg XI	$1s\ 2p\ ^3P_2 \rightarrow 1s^2\ ^1S_0$	6.80	0.42 ± 0.16	81.6	...
17b......	...	9.23	Mg XI	$1s\ 2p\ ^3P_1 \rightarrow 1s^2\ ^1S_0$	6.80	...	...	...
18........	9.31	9.31	Mg XI	$1s\ 2s\ ^3S_1 \rightarrow 1s^2\ ^1S_0$	6.80	0.69 ± 0.18	77.1	...
19a......	9.48	9.48	Fe XXI	$2s^2\ 2p\ 4d\ ^3D_1 \rightarrow 2s^2\ 2p^2\ ^3P_0$	7.05	0.27 ± 0.16	69.4	...
19b......	...	9.48	Ne X	$5p\ ^2P_{3/2} \rightarrow 1s\ ^2S_{1/2}$	6.80	...	...	...
19c......	...	9.48	Ne X	$5p\ ^2P_{1/2} \rightarrow 1s\ ^2S_{1/2}$	6.80	...	...	...
20a......	9.70	9.71	Ne X	$4p\ ^2P_{3/2} \rightarrow 1s\ ^2S_{1/2}$	6.80	0.99 ± 0.19	85.9	1
20b......	...	9.71	Ne X	$4p\ ^2P_{1/2} \rightarrow 1s\ ^2S_{1/2}$	6.80	...	...	...
21a......	9.96	9.97	Ni XXV	$2s\ 3d\ ^1D_2 \rightarrow 2s\ 2p\ ^1P_1$	7.30	0.21 ± 0.15	84.0	1
21b......	...	9.98	Ni XIX	$2p^5\ 4d\ ^1P_1 \rightarrow 2p^6\ ^1S_0$	6.90	...	...	...
22a......	10.02	10.02	Na XI	$2p\ ^2P_{3/2} \rightarrow 1s\ ^2S_{1/2}$	6.90	0.61 ± 0.17	86.5	1
22b......	...	10.03	Na XI	$2p\ ^2P_{1/2} \rightarrow 1s\ ^2S_{1/2}$	6.90	...	...	...
23a......	10.24	10.24	Ne X	$3p\ ^2P_{3/2} \rightarrow 1s\ ^2S_{1/2}$	6.80	1.36 ± 0.21	81.6	1
23b......	...	10.24	Ne X	$3p\ ^2P_{1/2} \rightarrow 1s\ ^2S_{1/2}$	6.80	...	...	...
24........	10.62	10.62	Fe XXIV	$1s^2\ 3p\ ^2P_{3/2} \rightarrow 1s^2\ 2s\ ^2S_{1/2}$	7.30	0.97 ± 0.19	72.1	1
25........	10.66	10.66	Fe XXIV	$1s^2\ 3p\ ^2P_{1/2} \rightarrow 1s^2\ 2s\ ^2S_{1/2}$	7.30	0.63 ± 0.18	71.4	1
26........	10.98	10.98	Fe XXIII	$2s\ 3p\ ^1P_1 \rightarrow 2s^2\ ^1S_0$	7.20	0.83 ± 0.18	63.4	1
27a......	11.02	11.02	Fe XXIII	$2s\ 3p\ ^3P_1 \rightarrow 2s^2\ ^1S_0$	7.20	1.06 ± 0.19	62.5	1
27b......	...	11.03	Fe XXIV	$1s^2\ 3d\ ^2D_{3/2} \rightarrow 1s^2\ 2p\ ^2P_{1/2}$	7.30	...	...	...
28a......	11.18	11.17	Fe XXIV	$1s^2\ 3d\ ^2D_{5/2} \rightarrow 1s^2\ 2p\ ^2P_{3/2}$	7.30	0.87 ± 0.19	56.9	1
28b......	...	11.19	Fe XXIV	$1s^2\ 3d\ ^2D_{3/2} \rightarrow 1s^2\ 2p\ ^2P_{3/2}$	7.30	...	...	...
29........	11.43	11.43	Fe XXIV	$1s^2\ 3s\ ^2S_{1/2} \rightarrow 1s^2\ 2p\ ^2P_{3/2}$	7.30	0.59 ± 0.18	55.5	1
30a......	11.44	11.44	Fe XXIII	$2s\ 3d\ ^3D_3 \rightarrow 2s\ 2p\ ^3P_2$	7.15	0.40 ± 0.17	55.2	1
30b......	...	11.44	Fe XXII	$2s\ 2p(^3P)3p\ ^4S_{3/2} \rightarrow 2s^2\ 2p\ ^2P_{1/2}$	7.10	...	...	...
31........	11.54	11.55	Ne IX	$1s\ 3p\ ^1P_1 \rightarrow 1s^2\ ^1S_0$	6.60	0.57 ± 0.16	53.5	1
32........	11.74	11.74	Fe XXIII	$2s\ 3d\ ^1D_2 \rightarrow 2s\ 2p\ ^1P_1$	7.20	1.26 ± 0.21	49.9	1
33........	11.77	11.77	Fe XXII	$2s^2\ (^1S)\ 3d\ ^2D_{3/2} \rightarrow 2s^2\ 2p\ ^2P_{1/2}$	7.10	1.28 ± 0.21	49.4	1
34a......	11.93	11.92	Fe XXII	$2s^2\ (^1S)\ 3d\ ^2D_{5/2} \rightarrow 2s^2\ 2p\ ^2P_{3/2}$	7.10	0.46 ± 0.15	47.0	1
34b......	...	11.93	Fe XXII	$2s^2\ (^1S)\ 3d\ ^2D_{3/2} \rightarrow 2s^2\ 2p\ ^2P_{3/2}$	7.10	...	...	...
34c......	...	11.94	Fe XXI	$2s\ 2p^2\ (^4P)\ 3p\ ^3D_1 \rightarrow 2s^2\ 2p^2\ ^3P_0$	7.10	...	...	...
35a......	12.13	12.12	Fe XVII	$2p^5\ 4d\ ^1P_1 \rightarrow 2p^6\ ^1S_0$	6.80	7.13 ± 0.37	42.6	1, 2
35b......	...	12.13	Ne X	$2p\ ^2P_{3/2} \rightarrow 1s\ ^2S_{1/2}$	6.80	...	...	...
35c......	...	12.14	Ne X	$2p\ ^2P_{1/2} \rightarrow 1s\ ^2S_{1/2}$	6.80	...	...	...
36........	12.27	12.26	Fe XVII	$2p^5\ 4d\ ^3D_1 \rightarrow 2p^6\ ^1S_0$	6.80	0.74 ± 0.19	41.3	1
37........	12.29	12.28	Fe XXI	$2s^2\ 2p\ 3d\ ^3D_1 \rightarrow 2s^2\ 2p^2\ ^3P_0$	7.00	1.06 ± 0.20	41.1	1, 2
38a......	12.83	12.82	Fe XX	$2s^2\ 2p^2(^3P)3d\ ^4P_{5/2} \rightarrow 2s^2\ 2p^3\ ^4S_{3/2}$	7.00	1.18 ± 0.18	35.0	1
38b......	...	12.82	Fe XX	$2s^2\ 2p^2(^3P)3d\ ^4P_{3/2} \rightarrow 2s^2\ 2p^3\ ^4S_{3/2}$	7.00	...	...	...
38c......	...	12.82	Fe XXI	$2s\ 2p^2(^4P)3d\ ^3P_2 \rightarrow 2s\ 2p^3\ ^3D_1$	7.00	...	...	...
38d......	...	12.83	Fe XX	$2s^2\ 2p^2(^3P)3d\ ^4P_{1/2} \rightarrow 2s^2\ 2p^3\ ^4S_{3/2}$	7.00	...	...	...

TABLE 1—*Continued*

Label	λ_{obs}[a] (Å)	λ_{pred}[a] (Å)	Ion	Transition (upper → lower)	$\log T_{max}$[b] (K)	(Count Rates $\pm\,\sigma$)[c] (counts ks^{-1})	Effective Area[d] (cm^2)	EM(T)[e]
39a......	13.45	13.45	Ne IX	$1s\,2p\ ^1P_1 \rightarrow 1s^2\ ^1S_0$	6.60	1.74 ± 0.24	28.4	1, 2
39b......	...	13.46	Fe XIX	$2p^3(^2D)3d\ ^3D_1 \rightarrow 2s^2\ 2p^4\ ^3P_0$	6.90	...	...	...
39c......	...	13.46	Fe XIX	$2p^3(^2D)3d\ ^3S_1 \rightarrow 2s^2\ 2p^4\ ^3P_2$	6.90	...	...	...
40a......	13.51	13.51	Fe XXI	$2s\,2p^2(^4P)3s\ ^3P_0 \rightarrow 2s\,2p^3\ ^3D_1$	7.00	1.30 ± 0.19	27.8	1
40b......	...	13.52	Fe XIX	$2p^3(^2D)3d\ ^3D_3 \rightarrow 2s^2\ 2p^4\ ^3P_2$	6.90	...	...	...
40c......	...	13.53	Fe XIX	$2p^3(^2D)3d\ ^3D_2\ \rightarrow\ 2s^2\ 2p^4\ ^3P_2$	6.90	...	...	...
41a......	13.55	13.55	Fe XIX	$2p^3(^2P)3d\ ^3D_2 \rightarrow 2s^2\ 2p^4\ ^3P_1$	6.90	0.46 ± 0.15	27.4	...
41b......	...	13.55	Ne IX	$1s\,2p\ ^3P_1 \rightarrow 1s^2\ ^1S_0$	6.55	...	...	...
41c......	...	13.57	Fe XIX	$2p^3(^2D)3d\ ^3P_2 \rightarrow 2s^2\ 2p^4\ ^3P_2$	6.90	...	...	...
41d......	...	13.57	Fe XXI	$2s^2\ 2p\,3p\ ^1S_0 \rightarrow 2s\,2p^3\ ^3D_1$	7.00	...	...	...
42a......	13.70	13.70	Ne IX	$1s\,2s\ ^3S_1 \rightarrow 1s^2\ ^1S_0$	6.60	0.98 ± 0.18	23.9	...
42b......	...	13.70	Fe XIX	$2p^3(^2D)3d\ ^3D_2 \rightarrow 2s^2\ 2p^4\ ^3P_1$	6.90	...	...	...
42c......	...	13.70	Fe XIX	$2p^3(^2P)3d\ ^3D_2 \rightarrow 2s^2\ 2p^4\ ^1D_2$	6.90	...	...	...
43a......	14.21	14.20	Fe XVIII	$2p^4(^1D)3d\ ^2D_{5/2} \rightarrow 2s^2\ 2p^5\ ^2P_{3/2}$	6.90	1.51 ± 0.20	22.7	1, 2
43b......	...	14.21	Fe XVIII	$2p^4(^1D)3d\ ^2P_{3/2} \rightarrow 2s^2\ 2p^5\ ^2P_{3/2}$	6.90	...	...	...
44a......	14.27	14.26	Fe XVIII	$2p^4(^1D)3d\ ^2S_{1/2} \rightarrow 2s^2\ 2p^5\ ^2P_{3/2}$	6.90	0.37 ± 0.14	25.1	1
44b......	...	14.27	Fe XVIII	$2p^4(^1D)3d\ ^2F_{5/2} \rightarrow 2s^2\ 2p^5\ ^2P_{3/2}$	6.90	...	...	...
44c......	...	14.27	Fe XX	$2s\,2p^3(^5S)3s\ ^4S_{3/2} \rightarrow 2s\,2p^4\ ^4P_{5/2}$	7.00	...	...	...
45a......	14.37	14.36	Fe XVIII	$2p^4(^1D)3d\ ^2D_{3/2} \rightarrow 2s^2\ 2p^5\ ^2P_{1/2}$	6.90	0.52 ± 0.15	25.3	1
45b......	...	14.37	Fe XVIII	$2p^4(^3P)3d\ ^2D_{5/2} \rightarrow 2s^2\ 2p^5\ ^2P_{3/2}$	6.90	...	...	...
46........	14.53	14.53	Fe XVIII	$2p^4(^3P)3d\ ^2F_{5/2} \rightarrow 2s^2\ 2p^5\ ^2P_{3/2}$	6.90	0.33 ± 0.13	24.2	1
47........	14.55	14.55	Fe XVIII	$2p^4(^3P)3d\ ^4P_{3/2} \rightarrow 2s^2\ 2p^5\ ^2P_{3/2}$	6.90	0.18 ± 0.13	24.0	1
48a......	14.60	14.58	Fe XVIII	$2p^4(^3P)3d\ ^4P_{1/2} \rightarrow 2s^2\ 2p^5\ ^2P_{3/2}$	6.90	0.19 ± 0.12	23.4	...
48b......	...	14.61	Fe XVIII	$2p^4(^3P)3d\ ^2P_{3/2} \rightarrow 2s^2\ 2p^5\ ^2P_{1/2}$	6.90	...	...	...
49a......	14.67	14.67	Fe XIX	$2p^3(^2D)3s\ ^3D_3 \rightarrow 2s^2\ 2p^4\ ^3P_2$	6.90	0.27 ± 0.13	23.7	1
49b......	...	14.67	Fe XVIII	$2p^4(^3P)3d\ ^2D_{3/2} \rightarrow 2s^2\ 2p^5\ ^2P_{1/2}$	6.90	...	...	...
50........	15.01	15.02	Fe XVII	$2p^5\ 3d\ ^1P_1 \rightarrow 2p^6\ ^1S_0$	6.75	1.85 ± 0.23	19.4	1, 2
51........	15.08	15.08	Fe XIX	$2s\,2p^4(^4P)3s\ ^3P_2 \rightarrow 2s\,2p^5\ ^3P_2$	6.90	0.31 ± 0.13	20.0	1
52a......	15.18	15.18	O VIII	$4p\ ^2P_{3/2} \rightarrow 1s\ ^2S_{1/2}$	6.50	0.29 ± 0.13	19.5	1
52b......	...	15.18	O VIII	$4p\ ^2P_{1/2} \rightarrow 1s\ ^2S_{1/2}$	6.50	...	...	...
52c......	...	15.20	Fe XIX	$2p^3(^4S)3s\ ^5S_2 \rightarrow 2s^2\ 2p^4\ ^3P_2$	6.90	...	...	...
53........	15.26	15.26	Fe XVII	$2p^5\ 3d\ ^3D_1 \rightarrow 2p^6\ ^1S_0$	6.75	0.44 ± 0.14	18.1	1
54a......	16.00	16.00	Fe XVIII	$2p^4(^3P)3s\ ^2P_{3/2} \rightarrow 2s^2\ 2p^5\ ^2P_{3/2}$	6.90	1.00 ± 0.17	16.4	1
54b......	...	16.01	O VIII	$3p\ ^2P_{3/2} \rightarrow 1s\ ^2S_{1/2}$	6.50	...	...	...
54c......	...	16.01	O VIII	$3p\ ^2P_{1/2} \rightarrow 1s\ ^2S_{1/2}$	6.50	...	...	...
55........	16.08	16.07	Fe XVIII	$2p^4(^3P)3s\ ^4P_{5/2} \rightarrow 2s^2\ 2p^5\ ^2P_{3/2}$	6.90	0.52 ± 0.14	16.1	1
56........	16.11	16.12	Fe XIX	$2p^3(^2D)3p\ ^3P_2 \rightarrow 2s\,2p^5\ ^3P_2$	6.90	0.04 ± 0.09	16.0	...
57........	16.16	16.17	Fe XVIII	$2s\,2p^5(^3P)3s\ ^2P_{3/2} \rightarrow 2s\,2p^6\ ^2S_{1/2}$	6.90	0.25 ± 0.12	15.7	1
58........	16.77	16.78	Fe XVII	$2p^5\ 3s\ ^3P_1 \rightarrow 2p^6\ ^1S_0$	6.70	0.83 ± 0.16	12.4	1
59........	17.05	17.05	Fe XVII	$2p^5\ 3s\ ^1P_1 \rightarrow 2p^6\ ^1S_0$	6.70	0.96 ± 0.17	11.7	1
60........	17.09	17.10	Fe XVII	$2p^5\ 3s\ ^3P_2 \rightarrow 2p^6\ ^1S_0$	6.70	0.91 ± 0.17	11.1	1
61a......	18.97	18.97	O VIII	$2p\ ^2P_{3/2} \rightarrow 1s\ ^2S_{1/2}$	6.50	2.44 ± 0.24	7.2	1, 2
61b......	...	18.97	O VIII	$2p\ ^2P_{1/2} \rightarrow 1s\ ^2S_{1/2}$	6.50	...	...	...
62........	21.60	21.60	O VII	$1s\,2p\ ^1P_1 \rightarrow 1s^2\ ^1S_0$	6.30	0.13 ± 0.10	3.3	1, 2
63a......	24.77	24.78	N VII	$2p\ ^2P_{3/2} \rightarrow 1s\ ^2S_{1/2}$	6.30	0.12 ± 0.10	3.0	1
63b......	...	24.78	N VII	$2p\ ^2P_{1/2} \rightarrow 1s\ ^2S_{1/2}$	6.30	...	...	...

[a] Observed and predicted (CHIANTI database) wavelengths. In the cases of unresolved blends, identified by the same label number, we list the main components in order of increasing predicted wavelength.

[b] Temperature of maximum emissivity.

[c] Count rates with uncertainties at the 68% confidence level. In the cases of unresolved blends, identified by the same label number, we report only the total line count rates.

[d] MEG first-order effective area, needed to convert the measured count rate to flux.

[e] Lines selected to derive the emission measure distribution with approach 1 or 2.

proposed by Kashyap & Drake (1998), which performs a search in the EM(T) parameter space using a Monte Carlo Markov chain method, with the aim of maximizing the probability of obtaining equal model and observed line fluxes. Moreover, we have also used two different methods for the abundance determination so that the two approaches are effectively independent. One of the aims of this is to compare the results from the different approaches in order to find which results are the least affected by the methods and hence more

robust. Hereafter, we will refer to the first selection as approach 1, and to the second as approach 2.

3.1.1. *Approach 1*

The first approach is based on the use of all lines strong enough to yield a useful flux measurement and that are also reasonably isolated, density independent, and not affected by identification problems. With this choice, the EM(T) analysis is based on the most reliable line fluxes among those

measured. Note that for a solar abundance corona this selection criterion will produce a set of measurements mainly composed of iron lines. For the MEG spectrum of PZ Tel, the lines included in this selection are indicated in the last column of Table 1.

With this choice we are able to derive, besides the $EM(T)$, the abundances relative to that of iron of all the chemical elements for which at least one line has been included in the selection. The abundance reconstruction is performed simultaneously with the $EM(T)$ as follows: we first used only the selected iron lines to obtain an initial $EM(T)$; we then added lines of other elements, one element at a time, in order to obtain a new $EM(T)$ and the abundances of the involved elements relative to Fe. At each step, we kept the previous set of $EM(T)$ and abundances as the starting point for the new reconstruction. The sequence of elements has been established in order to gradually extend the temperature range where the $EM(T)$ is constrained. Finally, the Fe abundance has been evaluated by comparing the observed continuum with the predictions based on different metallicity values (see Argiroffi et al. 2003 for more details).

In principle, this selection criterion allows us to reach the finest temperature resolution in the $EM(T)$ because of the large number of lines involved. While many of the lines have emissivity functions that peak at the same T_{max}, these emissivity functions can have significantly different shapes and hence can provide more information on the structure of the $EM(T)$ than a single line at the same temperature. Of course, this assumption does depend on there not being significant errors in the emissivity functions of the included lines that might instead lead to distortions of the derived $EM(T)$ relative to its true form.

3.1.2. Approach 2

The second approach is based on the use of lines produced by He- and H-like ions and has been proposed by Schmitt & Ness (2004) and J. J. Drake (2004, in preparation). This choice is motivated by the simplicity of these ions and the fact that they are likely to have more reliable emissivity functions than lines produced by ions with a larger number of electrons, and in particular the Fe lines. Note that by adopting this selection it becomes necessary to separate the $EM(T)$ reconstruction from the abundance evaluation because these quantities are more critically correlated than in the case of approach 1. This is because there is no element, such as iron in approach 1, whose lines cover the whole temperature range. In order to separate the $EM(T)$ and abundance reconstruction, we have used the flux *ratios* of the He-like triplet resonance line to the H-like Lyα line for each of the different elements for which these lines have been significantly detected. In addition to these line ratios, we have also included three prominent Fe lines for a better sampling of the temperature range. In the case of PZ Tel, the lines selected are marked in the last column of Table 1.

In applying this method, we also included measurements of the continuum flux at 2.4–3.4, 5.1–6.1, and 19–20 Å. Fluxes were obtained by summing the counts in each interval. We have checked that no strong line features were present in these intervals, in both the observed and predicted spectra. These continuum measurements serve two purposes. First, they provide additional temperature information, based on the falloff of the dominant bremsstrahlung continuum toward shorter wavelengths. Second, they provide a normalization for the $EM(T)$ since our approach based on line ratios described

above provides only an estimate of the *shape* of the function. An absolute measurement of $EM(T)$ also enables us to express element abundances relative to hydrogen. Element abundances were determined when a satisfactory $EM(T)$ had been derived by comparing predicted and observed line fluxes for each element.

This line-ratio method was developed by J. J. Drake (2004, in preparation) in order to investigate coronal element abundances in a large sample of stars. The H- and He-like resonance transitions of the abundant elements N, O, Ne, Mg, and Si are the brightest lines in coronal spectra and so should be detected in all stars for which well-exposed spectra have been obtained. Thus, one advantage of this method is that the same analysis using the same lines can be performed on many stars, limiting any systematic bias caused by star-to-star line selection differences. One disadvantage, at least in principle, is that the line emissivities of He- and H-like ions have in general a larger width in temperature than those of, for example, iron lines. Any fine structure in the $EM(T)$ function will therefore be more likely to be lost in this method than in an approach using a more extensive line list, such as our approach 1.

4. RESULTS

4.1. Emission Measure Distribution and Abundances

Considering the formation temperatures of the available spectral lines listed in Table 1, we have explored the $EM(T)$ in the $\log T$ range 6.0–7.5, with a bin size of $\Delta \log T = 0.1$.

In Figure 3, we show the $EM(T)$ obtained with the two different methods and line lists, while in Table 2 and Figure 4 we report the derived abundances. As explained in § 3.1, approach 1 compares the observed and predicted continuum level in order to evaluate the iron abundance and hence the overall plasma metallicity. Thus, we have not assigned an error bar to the Fe abundance in Figure 4. This comparison yields an iron abundance of ~0.3 times the currently accepted solar value (Grevesse & Sauval 1998). Note that the iron abundance so derived plays the role of a global factor both in the $EM(T)$ and in the abundance values derived with approach 1.

The O, Ne, Mg, Al, Si, S, and Fe abundance estimations in approach 2 were performed using the lines that were used in
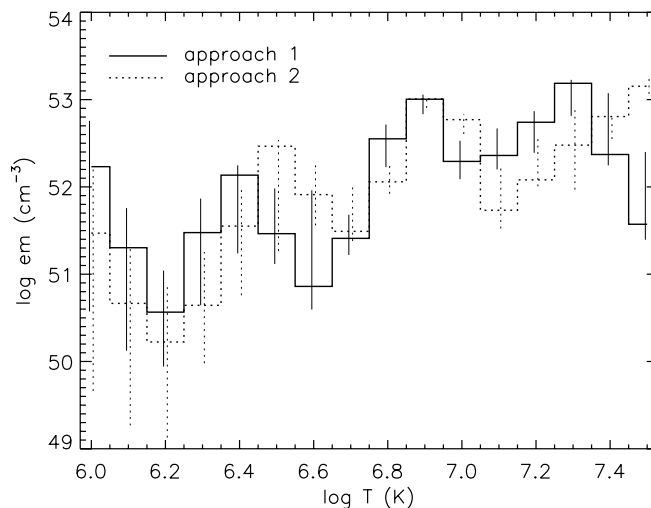

Fig. 3.—Emission measure distribution $EM(T)$ of PZ Tel derived with the two criteria introduced in § 3.1.

TABLE 2

ELEMENT ABUNDANCES $A_X = N_X/N_H$

ELEMENT	APPROACH 1		APPROACH 2	
	$A_X/A_{X_\odot}$	A_X	$A_X/A_{X_\odot}$	A_X
Na..................	1.2 ± 0.4	$(2.6 \pm 0.9) \times 10^{-6}$	1.5 ± 0.4	$(3.3 \pm 1.0) \times 10^{-6}$
Al..................	≤ 0.3	$\leq 1.0 \times 10^{-6}$	0.6 ± 0.3	$(1.7 \pm 0.7) \times 10^{-6}$
Ni..................	≤ 0.5	$\leq 9.5 \times 10^{-7}$	0.5 ± 0.4	$(9 \pm 6) \times 10^{-7}$
Mg.................	0.28 ± 0.03	$(1.1 \pm 0.1) \times 10^{-5}$	0.34 ± 0.03	$(1.3 \pm 0.1) \times 10^{-5}$
Fe..................	~ 0.3	$\sim 9.7 \times 10^{-6}$	0.27 ± 0.03	$(8.5 \pm 0.9) \times 10^{-6}$
Si	0.22 ± 0.03	$(7.9 \pm 0.9) \times 10^{-6}$	0.30 ± 0.04	$(1.1 \pm 0.1) \times 10^{-5}$
S	0.27 ± 0.10	$(6 \pm 2) \times 10^{-6}$	0.38 ± 0.13	$(8 \pm 3) \times 10^{-6}$
O...................	0.47 ± 0.06	$(3.1 \pm 0.4) \times 10^{-4}$	0.41 ± 0.08	$(2.7 \pm 0.5) \times 10^{-4}$
N...................	≤ 1.1	$\leq 9.4 \times 10^{-5}$	≤ 1.2	$\leq 9.7 \times 10^{-5}$
Ne..................	0.57 ± 0.04	$(6.9 \pm 0.5) \times 10^{-5}$	0.76 ± 0.06	$(9.1 \pm 0.8) \times 10^{-5}$

the EM(T) derivation; the N, Na, and Ni abundances were instead evaluated using their measured line counts listed in Table 1 that were excluded from the EM(T) analysis.

The two emission measure distributions obtained with the two approaches (see §§ 3.1.1 and 3.1.2) are compatible within statistical uncertainties in almost all the bins of the explored temperature range. Both EM(T) distributions show a maximum at log $T = 6.9$, which is a common feature for active stars (e.g., Drake 1996; Sanz-Forcada et al. 2003a), and also a significant emission measure for log $T \geq 7$. However, some differences are present, mainly near log $T \sim 6.5$ and in the high-temperature tails of the distributions.

Several causes might be responsible for these differences. Errors in the atomic data may yield different solutions if different line sets are used. This is one of the primary motives of our approach 2, which should introduce minimal errors arising from atomic data.

Another problem is due to the fact that the observed line fluxes are related to the EM(T) function through a Fredholm equation of the first type, which has no unique solution (e.g., Craig & Brown 1976). Different EM(T) and abundance sets might then reproduce equally well the observed line fluxes within measurement uncertainties. This nonuniqueness might also be affected by the resolution and amplitude of the temperature grid assumed a priori for the EM(T) reconstruction.
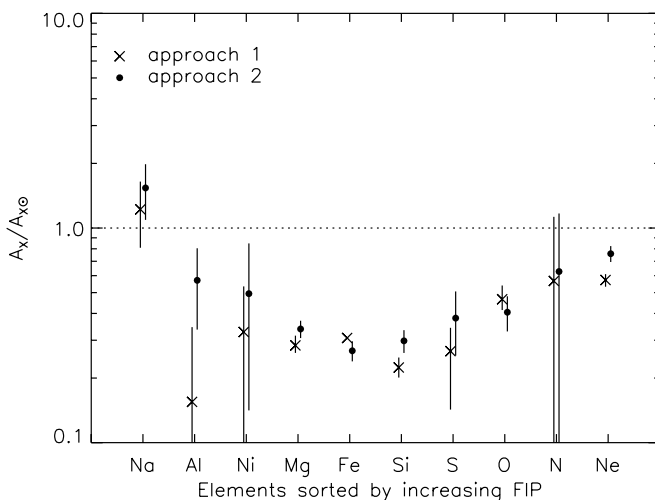

FIG. 4.—Abundances in solar units (Grevesse & Sauval 1998) vs. elements sorted by increasing FIP for both the criteria.

The two different line choices and methods provide consistent abundance values in most cases, indicating that the derived abundances do not depend on small differences in the emission measure distributions. We find a significant discrepancy between the two models only for Si and Ne abundances. These small abundance differences are probably due to the slightly different values of the EM(T) obtained with the two approaches in the temperature range where Si and Ne lines are produced.

In Figures 5 and 6, we show the comparison between observed and predicted line fluxes for both the solutions. From these plots we deduce that, as expected, the EM(T) derived with approach 1 shows a better overall description of the observed line fluxes of PZ Tel than in the other case but the predicted line flux values of the resonance line of the He-like ions and the Lyα line of the H-like ions are more discrepant than those computed with the approach 2 solution (Figs. 5 and 6, *filled circles*). Moreover, we note that the approach 2 solution describes spectral features formed at lower temperatures somewhat better, as represented by a smaller spread between observed and predicted fluxes for log $T \leq 7.0$. On the other hand, the approach 1 solution shows a smaller spread between observed and predicted fluxes for log $T \geq 7.0$.

Figure 4 shows that the PZ Tel coronal abundances, relative to solar photospheric values (Grevesse & Sauval 1998), do not show a strong FIP dependence but rather show a pattern versus FIP similar to that of other active stars (e.g., Brinkman et al. 2001; Drake et al. 2001; Audard et al. 2003; Sanz-Forcada et al. 2003b): elements at low and high FIP appear enhanced with respect to the medium-FIP elements. It is worth noting that we cannot compute abundance ratios relative to photospheric values because those of PZ Tel are not known; therefore, the *real* abundance-versus-FIP pattern may differ significantly from the one plotted in Figure 4 (e.g., Sanz-Forcada et al. 2004).

Finally we note that, using the flux measured for the Na XI Lyα line at 10.02 Å, we have performed what is to our knowledge the first coronal Na abundance estimate based on X-ray spectra. The Na abundance is useful for constraining the abundance-versus-FIP pattern at low FIP. The identification and subsequent flux estimation of these lines is nontrivial because this spectral region also contains a number of Fe XX and other lines. Ayres et al. (2001) and Phillips et al. (2001) identified the Na XI Lyα line in the HETGS spectra of HR 1099 and Capella, respectively. Sanz-Forcada et al. (2003b, 2004), in the HETGS of AB Dor and λ And, respectively, measured
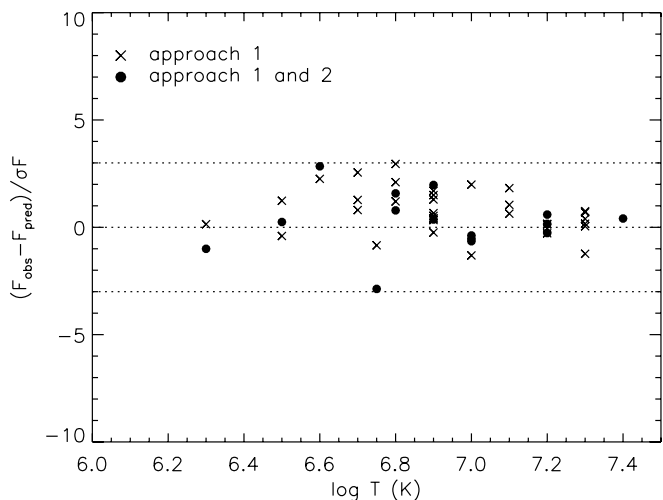
Fig. 5.—Comparison between observed line fluxes and those predicted by the EM(T) obtained with approach 1. We indicate with the crosses the line fluxes selected for approach 1 and not for approach 2, while the filled circles represent the line fluxes included both in approach 1 and 2.
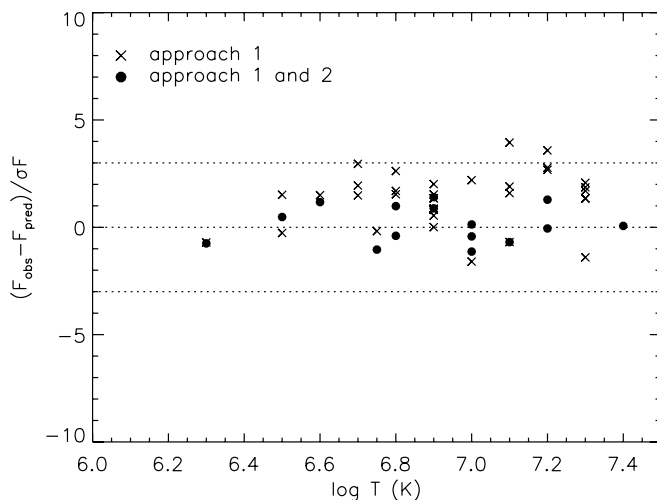

Fig. 6.—Comparison between observed line fluxes and those predicted by the EM(T) obtained with approach 2. The crosses and filled circles are as in Fig. 5.

the flux of a spectral feature at 10.02 Å but did not identify it because of a lack of Na lines in the Astrophysical Plasma Emission Database (APED). Moreover, in the HETGS spectrum of AR Lac, analyzed by Huenemoerder et al. (2003) using APED, this emission line at 10.02 Å is clearly visible and does not appear to be easily attributable to other species, such as Fe xx. In conclusion, we suggest that the spectral feature at 10.02 Å observed in several coronal X-ray spectra is to be identified with the Na xi Lyα line listed in the CHIANTI database.

4.2. *Electron Density*

Estimates of the electron density N_e can be obtained using He-like triplets (Gabriel & Jordan 1969). These spectral features consist of three lines (resonance r, intercombination i, and forbidden f) produced by transitions from $n = 2$ to $n = 1$ levels in He-like ions. For the physical conditions of coronal plasmas, the ratio f/i is predominantly sensitive to density, while the ratio $(i + f)/r$ is predominantly sensitive to temperature. Note that the density and the temperature inferred from these lines will be weighted averages of the region in which the relevant triplet is formed.

We have identified and measured in the MEG spectrum of PZ Tel the He-like triplets of Ne ix, Mg xi, and Si xiii ions, while for the O vii, Al xii, and S xv ions only the resonance line is measurable (see Table 1). In Table 3, we report the f/i ratios, together with the derived electron densities N_e and 1 σ uncertainties. Note that, because of the unresolved blends of Ne ix i and f lines with Fe xix lines, we have evaluated the Ne ix f/i ratio by subtracting the predicted fluxes of the Fe xix lines from the measured values. We have obtained density

values from Mg xi, while from Ne ix and Si xiii we have derived only an upper limit. We also point out here that our measured f/i ratios have uncertainties of more than 40% and are all consistent with their respective low-density limits at the 2 σ level.

5. DISCUSSION AND CONCLUSIONS

It is interesting to compare the coronal properties of PZ Tel found here with those of TW Hya and AB Dor, which are slightly younger and older, respectively, than PZ Tel. TW Hya is a classical T Tauri star with a circumstellar disk and an age of ~10 Myr (Webb et al. 1999). AB Dor is a K1 single star that has almost arrived on the main sequence. Collier Cameron & Foing (1997) have estimated the age of AB Dor to be in the range 20–30 Myr, while Favata et al. (1998) derived a slightly older age of about ≳35 Myr. In Figure 7, we show the positions on the H-R diagram of these three stars and have also superposed the evolutionary tracks from Ventura et al.
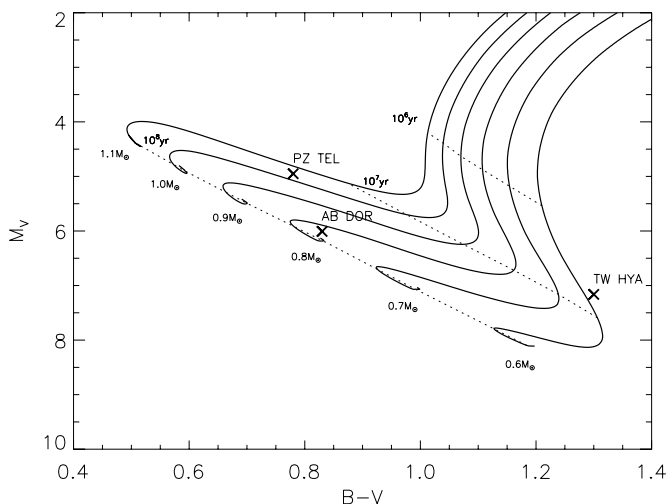
TABLE 3
Electron Densities Calculated from the He-like Triplets

Ion	$\log T_{max}$	f/i	$\log N_e$ (cm^{-3})
Ne ix....................................	6.6	3.0 ± 1.4	<11.8
Mg xi....................................	6.8	1.7 ± 0.8	12.6 ± 0.6
Si xiii	7.0	3.5 ± 2.1	<13.5

Fig. 7.—H-R diagram for PZ Tel, TW Hya, and AB Dor. Solid lines represent the evolutionary tracks of Ventura et al. (1998) evaluated for $Z = 0.01$. Dotted lines represent the isochrones at 10^6, 10^7, and 10^8 yr.

(1998) with $Z = 0.01$. The values of M_V and $B-V$ have been derived from the *Hipparcos* catalog (Perryman et al. 1997). Note however that TW Hya cannot be placed accurately on the H-R diagram because of the large variability observed in its color indices (Rucinski & Krautter 1983; Mekkaden 1998). Rucinski & Krautter (1983) found that the spectrum of TW Hya is compatible with a K7 V star, and we have therefore assumed a $B-V$ color index of 1.30 (Johnson 1966). The positions of these stars on the H-R diagram (Fig. 7) confirm that TW Hya and AB Dor are in evolutionary stages just preceding and following the stage of PZ Tel.

The coronal emission of TW Hya and AB Dor has been studied via *Chandra* HETGS observations by Kastner et al. (2002), Sanz-Forcada et al. (2003b), and D. García-Alvarez (2004, in preparation). Comparison with our present results shows that PZ Tel is very similar to AB Dor in its emission measure distribution, element abundances, and electron densities. TW Hya, however, appears to be very different in many respects. Its emission measure distribution peaks at $\log T = 6.5$ and there is no evidence of plasma at $\log T \geq 7.0$ in the observed spectrum, while PZ Tel and AB Dor have their maxima at $\log T = 6.9$ and both exhibit considerable emission measure at higher temperatures. There are also abundance differences, especially regarding the Ne/Fe ratio. In TW Hya, Ne/Fe is larger than the solar value by a factor of ~ 10, whereas for AB Dor and PZ Tel the enhancements are less extreme, with factors of ~ 5 and ~ 2, respectively.[5]

Finally, the electron densities of the emitting plasma of TW Hya, derived from the O VII and Ne IX He-like triplets, turn out to be much higher than those of PZ Tel and AB Dor. The differences in densities between PZ Tel, AB Dor, and TW Hya can be appreciated in Figure 8, where we show their observed MEG spectra in the region of the Ne IX lines. We show the Ne IX triplet region because it is the only triplet for which the observed spectra have sufficient S/N for all three stars (in fact, the O VII intercombination and forbidden lines in the spectrum of PZ Tel are not measurable). It is known that the Ne IX triplet is complicated by blends with highly ionized Fe lines that are clearly visible in the PZ Tel spectrum, e.g., at 13.51 Å (see also Table 1 for more detail). The Fe XIX line at ~ 13.51 Å in the TW Hya spectrum is instead not observable because of the peculiar Ne/Fe abundance ratio and the relatively low temperature of the peak in EM(T) for this star. However, it is still quite clear that the relative intensities of the i and f lines for PZ Tel and AB Dor are very different from those of TW Hya. In fact, the f/i ratio is 2.9 ± 0.3 for AB Dor, 3.0 ± 1.4 for PZ Tel, and 0.44 ± 0.12 for TW Hya, implying electron density values of $\log N_e \sim 11$, < 12, and ~ 13, respectively.

As noted in § 1, Kastner et al. (2002) attributed the dominance of plasma at a temperature of 3×10^6 K, with high electron densities of order $\log N_e \sim 13$ in TW Hya, to accretion rather than a magnetically heated corona. In the accretion scenario, the plasma is heated in a shock at the stellar surface. The strong difference we see here between the X-ray emission of the accreting TW Hya and nonaccreting PZ Tel supports these conclusions. However, there are two outstanding questions that the accretion scenario does not answer: (1) why is the Ne/Fe abundance in the shocked plasma similar to that seen in some coronally active RS CVn systems (see, e.g.,
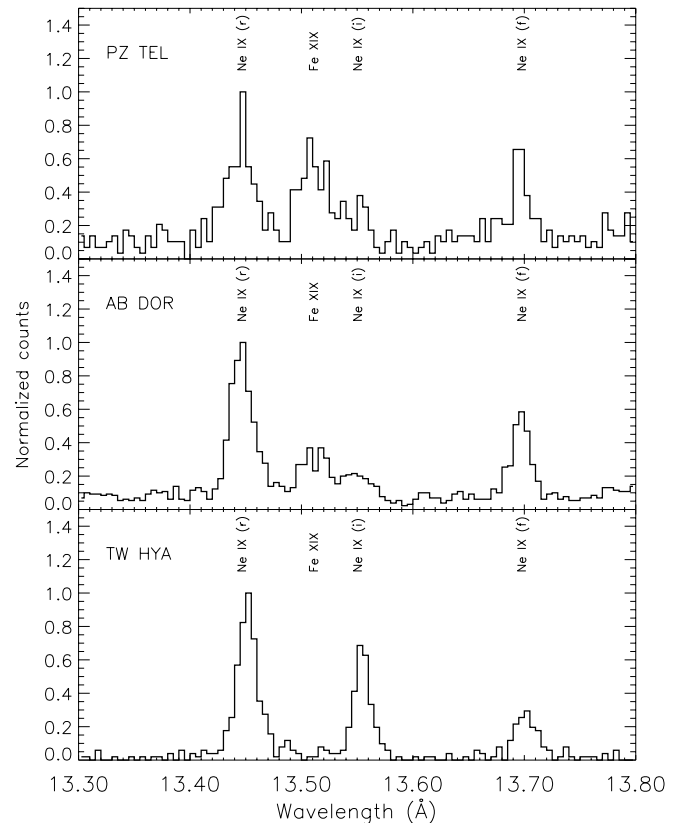

Fig. 8.—Comparison of the Ne IX spectral region of PZ Tel, AB Dor, and TW Hya. For each star, we have plotted the first-order spectra of *Chandra* MEG.

Drake et al. 2001; Huenemoerder et al. 2001) and so different from the presumed value in the accreting circumstellar material? And (2) why is there very little trace of underlying coronal activity similar to that in PZ Tel?

If the Ne/Fe abundance seen in TW Hya is indeed representative of the accreting material, then significant compositional fractionation must be occurring in the circumstellar disk or in the inner disk-magnetosphere region from which the accreting plasma falls onto the star. The lack or weakness of "normal" coronal activity on TW Hya might logically be associated with accretion activity or the presence of substantial disk material close in to the star itself. In this respect, however, it seems that TW Hya might be unusual among accreting CTTSs. X-ray studies at low resolution of large samples of PMS stars (Tsujimoto et al. 2002; Nakajima et al. 2003) have indicated that CTTSs coronal spectra tend to be dominated by plasma at $\log T \sim 7.5$, much hotter than in the case of TW Hya. Note however that CTTSs are often highly absorbed and therefore the high difference in temperature could be the result of a selection bias because of their distances larger than that of TW Hya.

Our study of PZ Tel shows it to be much more similar in EM(T), abundances, and electron densities to AB Dor than to TW Hya. Because PZ Tel is younger than AB Dor, our results indicate that coronal properties do not change appreciably during the evolution of PMS stars from the post–T Tauri phase to the main sequence. On the other hand, if TW Hya is assumed to be representative of CTTSs it follows that as soon as disk dissipation and significant accretion processes have ended the coronal structure quickly evolves to that of any other star of similar spectral type and rotation rate.

---

[5] For the Ne/Fe abundance ratio of PZ Tel, we have used results obtained with approach 1. Approach 2 gives a Ne/Fe abundance ratio ~ 3, which also tends to confirm the observed trend.

REFERENCES

Argiroffi, C., Maggio, A., & Peres, G. 2003, A&A, 404, 1033
Audard, M., Güdel, M., Sres, A., Raassen, A. J. J., & Mewe, R. 2003, A&A, 398, 1137
Ayres, T. R., Brown, A., Osten, R. A., Huenemoerder, D. P., Drake, J. J., Brickhouse, N. S., & Linsky, J. L. 2001, ApJ, 549, 554
Barnes, J. R., Collier Cameron, A., James, D. J., & Donati, J.-F. 2000, MNRAS, 314, 162
Brinkman, A. C., et al. 2001, A&A, 365, L324
Coates, D. W., Halprin, L., Sartori, P., & Thompson, K. 1980, Inf. Bull. Variable Stars, 1849, 1
Collier Cameron, A., & Foing, B. H. 1997, Observatory, 117, 218
Craig, I. J. D., & Brown, J. C. 1976, A&A, 49, 239
Drake, J. J. 1996, in ASP Conf. Ser. 109, Cool Stars, Stellar Systems, and the Sun, ed. R. Pallavicini & A. K. Dupree (San Fransisco: ASP), 203
———. 2002, in ASP Conf. Ser. 277, Stellar Coronae in the *Chandra* and *XMM-Newton* Era, ed. F. Favata & J. J. Drake (San Fransisco: ASP), 75
Drake, J. J., Brickhouse, N. S., Kashyap, V., Laming, J. M., Huenemoerder, D. P., Smith, R., & Wargelin, B. J. 2001, ApJ, 548, L81
Favata, F., Micela, G., Sciortino, S., & D'Antona, F. 1998, A&A, 335, 218
Feigelson, E. D., & Montmerle, T. 1999, ARA&A, 37, 363
Feldman, U. 1992, Phys. Scr., 46, 202
Flaccomio, E., Micela, G., & Sciortino, S. 2003, A&A, 402, 277
Flower, P. J. 1996, ApJ, 469, 355
Gabriel, A. H., & Jordan, C. 1969, MNRAS, 145, 241
Grevesse, N., & Sauval, A. J. 1998, Space Sci. Rev., 85, 161
Güdel, M., et al. 2001, A&A, 365, L336
Houk, N. 1978, Michigan Catalogue of Two-Dimensional Spectral Types for the HD Stars (Ann Arbor: Univ. Michigan)
Huenemoerder, D. P., Canizares, C. R., Drake, J. J., & Sanz-Forcada, J. 2003, ApJ, 595, 1131
Huenemoerder, D. P., Canizares, C. R., & Schulz, N. S. 2001, ApJ, 559, 1135
Innis, J. L., Coates, D. W., & Thompson, K. 1984, Proc. Astron. Soc. Australia, 5, 540
Innis, J. L., Thompson, K., & Coates, D. W. 1986, MNRAS, 223, 183

Johnson, H. L. 1966, ARA&A, 4, 193
Kashyap, V., & Drake, J. J. 1998, ApJ, 503, 450
———. 2000, BAAS, 32, 1227
Kastner, J. H., Huenemoerder, D. P., Schulz, N. S., Canizares, C. R., & Weintraub, D. A. 2002, ApJ, 567, 434
Mazzotta, P., Mazzitelli, G., Colafrancesco, S., & Vittorio, N. 1998, A&AS, 133, 403
Mekkaden, M. V. 1998, A&A, 340, 135
Mewe, R., Kaastra, J. S., White, S. M., & Pallavicini, R. 1996, A&A, 315, 170
Montmerle, T. 2002, in ASP Conf. Ser. 277, Stellar Coronae in the *Chandra* and *XMM-Newton* Era, ed. F. Favata & J. J. Drake (San Fransisco: ASP), 173
Nakajima, H., Imanishi, K., Takagi, S., Koyama, K., & Tsujimoto, M. 2003, PASJ, 55, 635
Perryman, M. A. C., et al. 1997, A&A, 323, L49
Phillips, K. J. H., Mathioudakis, M., Huenemoerder, D. P., Williams, D. R., Phillips, M. E., & Keenan, F. P. 2001, MNRAS, 325, 1500
Plucinsky, P. P., et al. 2003, Proc. SPIE, 4851, 89
Rucinski, S. M., & Krautter, J. 1983, A&A, 121, 217
Sanz-Forcada, J., Brickhouse, N. S., & Dupree, A. K. 2003a, ApJS, 145, 147
Sanz-Forcada, J., Favata, F., & Micela, G. 2004, A&A, 416, 281
Sanz-Forcada, J., Maggio, A., & Micela, G. 2003b, A&A, 408, 1087
Schmitt, J. H. M. M., & Ness, J.-U. 2004, A&A, 415, 1099
Soderblom, D. R., King, J. R., & Henry, T. J. 1998, AJ, 116, 396
Stelzer, B., & Neuhäuser, R. 2000, A&A, 361, 581
Stelzer, B., & Schmitt, J. H. M. M. 2004, A&A, in press
Tsujimoto, M., Koyama, K., Tsuboi, Y., Goto, M., & Kobayashi, N. 2002, ApJ, 566, 974
Ventura, P., Zeppieri, A., Mazzitelli, I., & D'Antona, F. 1998, A&A, 331, 1011
Webb, R. A., Zuckerman, B., Platais, I., Patience, J., White, R. J., Schwartz, M. J., & McCarthy, C. 1999, ApJ, 512, L63
Young, P. R., Del Zanna, G., Landi, E., Dere, K. P., Mason, H. E., & Landini, M. 2003, ApJS, 144, 135
Zuckerman, B., & Webb, R. A. 2000, ApJ, 535, 959